IEEE Access
Multidisciplinary | Rapid Review | Open Access Journal

Received August 9, 2021, accepted September 18, 2021, date of publication September 23, 2021, date of current version October 7, 2021.

Digital Object Identifier 10.1109/ACCESS.2021.3115253

Inversion of Volume Scattering Function for Estimation of Bubble Size Distribution in Ocean Waters

BHOGESWARA RAO ANGARA[1,2], PALANISAMY SHANMUGAM[1], AND HARISHANKAR RAMACHANDRAN[2]

[1]Department of Ocean Engineering, Indian Institute of Technology Madras, Chennai 600036, India
[2]Department of Electrical Engineering, Indian Institute of Technology Madras, Chennai 600036, India

Corresponding author: Palanisamy Shanmugam (pshanmugam@iitm.ac.in)

This work was supported in part by the Natural Resources Data Management System (NRDMS) of the Department of Science and Technology of the Government of India under Grant OEC1819150DSTXPSHA. The work of Bhogeswara Rao Angara was supported by the Indian Institute of Technology Madras through the Interdisciplinary Research Program (IDRP) and Scholarships offered by Ministry of Human Resource Development (MHRD).

ABSTRACT Angular distribution of the intensity of light scattered by a spherical air bubble in the oceanic medium is distinctive near the critical scattering angle region, when light interacts with a bubble with a refractive index less than its surrounding medium. This study is aimed at presenting theoretical and experimental results for the volume scattering function (VSF) of the bubbles generated under oceanic and laboratory conditions. The effect of bubbles on the VSFs was investigated using Mie calculations for the bubble sizes ranging from 5 to 200 μm and their size distribution slopes ranging from 3.6 to 4.6. Findings revealed that the critical angle scattering patterns (50°-80°) produced by bubbles become well-pronounced, enhanced and dependent on the minimum and maximum bubble sizes and their size distribution slopes (r_{min}, r_{max} and α). A relationship of the volume scattering phase function ($\tilde{\beta}(\theta, \lambda)$) between an inverse power-law and a normally-distributed bubble population was established based on experimental data. Both experimental results and Mie simulations showed that the angular position of the first critical dark fringe (θ_1) shifts in the direction of the critical angle as the minimum and mean values of the bubble size increase in accordance with the power law and normally-distributed bubble populations. The new inversion method predicted the light scattering patterns produced by bubbles near the critical angle region in close agreement with results from Mie theory simulations. The inversion method for estimating the bubble size distribution based on the measured VSF data have significant implications for underwater optical communication, imaging and ocean colour remote sensing studies.

INDEX TERMS Oceanic bubbles, volume scattering function, critical angle, inversion method, remote sensing.

I. INTRODUCTION

The study of light in the sea and its interactions with the particulates and bubbles are important for many subsea applications. This involves a better understanding of the absorption and scattering properties of water molecules, bubbles, and water constituents (phytoplankton, suspended sediments, detritus and dissolved organic matter) among other optical processes and feedback mechanisms. Considering the parallel rays falling upon a spherical bubble of radius greater than a few times the wavelength of incident light and according to the Geometric optics approximation theories, when the angle of incidence of a ray $\phi_c \geq \sin^{-1}(n_i/n_m)$, the ray is totally reflected (tunneling and surface curvature effects are ignored) due to the smaller refractive index of an air bubble ($n_i = 1.0003$) than the surrounding water medium ($n_m = 1.33257$) and the corresponding condition of the angle of scattering of a reflected ray is $\theta \leq \theta_c = 180 - 2\phi_c = 82.84°$ (because the refractive index of water is: n_m =1.33257, where θ_c is the critical scattering angle). If the angle of incidence of a ray is smaller than the ϕ_c, the ray will be reflected and refracted many times inside the bubble. The θ_c for bubbles may vary from 80° to 84° (refractive index of an air bubble, $m = n_i/n_m$, relative to that of the water, is

The associate editor coordinating the review of this manuscript and approving it for publication was Haiyong Zheng.

This work is licensed under a Creative Commons Attribution 4.0 License. For more information, see https://creativecommons.org/licenses/by/4.0/

within 0.740-0.769) because the refractive index of seawater depends on salinity and temperature and is a function of the wavelength of the incident ray.

The volume scattering function is a fundamental inherent optical property that describes the angular distribution of the scattered light. The scattered light intensity is dependent on the scattering angle and it becomes very distinctive near the critical scattering angle (θ_c) when light interacts with an air bubble with a refractive index (n_i) less than the surrounding water medium (n_m).

Studies on underwater detection, imaging, underwater wireless optical communication (UWOC) [1], satellite ocean color sensor design and its product evaluation [2], [3] are based on measurements of the inherent optical properties of bubbles in the upper ocean. The oceanic bubbles are abundantly produced by breaking waves near the sea surface [4], [5] and by moving ships [6]. A bubble number density frequently found at sea varies in the range from 10 to 150 μm. Among a large population of bubbles, larger bubbles of approximately 20 μm are frequently distributed in the surface layer and bubble sizes and concentrations decrease rapidly with depth [7]. At high wind speeds, small bubbles penetrate deep into the water column making a significant contribution to the total bubble population [8]. Bubble clouds also form whitecaps in near-surface water that have a marked effect on the inherent optical properties as well as on the magnitude and shape of visible light radiance or reflectance [9]–[12]. Bubbles entrained by breaking waves make a significantly larger contribution to the scattering coefficient and alter the upwelling radiance spectrum [3], [10].

The Lorenz-Mie Theory [13]–[15] provides a complete solution to Maxwell's equation that accurately predicts the light scattering properties of homogeneous spheres, such as a spherical bubble in water. For the past decades, several models have been developed to estimate the bubble size using a light scattering technique based on this theory [8], [16]–[19], despite some limitations associated with these models that the data be normally- and log-normally distributed [20]. The light absorption coefficient (a) of a bubbles within the blue-green portion is negligible, but it will become important with the organic coatings on the bubble surface and such organic coatings also exert a small influence on the scattering properties of coated bubbles with the higher refractive index [21]. Theoretical and experimental studies confirm that the critical-scattering angle (θ_c) of bubbles is up to about 80° to 84° (refractive index of bubbles, $m = n_i/n_m$, is about 0.740 to 0.769 relative to that of water) [22]–[24]. Because the critical-angle scattering by coated bubbles could be enhanced over the backward direction by a factor of 4-5 times, earlier studies have modelled and investigated the influence of organic-film-coated bubbles on the ocean colour remote sensing signals using the Mie theory [12], [21], [25], [26].

Numerous light scattering models were established and frequently used to characterize bubble size distributions in oceanic water. However, accurate prediction of bubble diameters in oceans has been a challenge for the available light-scattering models. More recently, several techniques have been developed to measure or predict the bubble size distribution in water, for example, laser diffraction scattering (LD) [27], static and dynamic light scattering (SLS, DLS), particle tracking analysis (PTA) [28], acoustic sensors [29], video imaging [30], and remote sensing techniques [31]. An inversion method was also developed based on the Critical Angle Refractometry and Sizing technique (CARS) [20], [32], [33] for the characterization of bubbly flows (size distribution and refractive index of bubbly flow). These methods also depend on the scattering behavior of bubbles near the critical angle and have disadvantages due to their requirement that the bubble size be normally- and log-normally distributed in the water.

Another inversion method based on the non-negatively constrained least squares and parameter choice was developed and tested using VSF measurement data [8], [16], [17], [34], [35]. This method attempts to invert the Fredholm equation to retrieve the composition and particle size distribution (e.g., algae, bubbles, sediment particles and detritus) from VSF data. The key assumption was that the particulates can be divided into sub-populations, each sub-population typically follows a log-normal distribution and the cumulative distribution of sub-populations also follows a power law. Previous experimental results work on the VSF and scattered light intensity near the critical angle confirm that the bubble size distributions generally follow a power law for the bubble sizes ranging from 0.5 to 125 μm [8].

The present study builds upon many theoretical and experimental works and analyzes the light scattering behavior exhibited by the oceanic bubbles (whose size distribution follows a power law) near the critical-angle. An Extensive computational work is performed in this study and it provides the scattered intensity, volume scattering function (VSF) and scattering coefficients of bubbles using Mie theory calculations. Finally, an inversion method is developed for estimating the bubble size distribution in oceanic water.

II. METHODOLOGY

A. MIE SCATTERING THEORY CALCULATIONS

The Mie-scattering theory gives a rigorous solution of Maxwell's equations for the scattering of a plane wave and is generally applicable for all oceanic materials. The Mie-scattering calculation is used to compute the scattering by spheres of arbitrary size with the effect of the refractive index of bubbles. According to this theory, the incident, internal and external (scattered) fields are expanded in radiating vector spherical harmonics using the Bessel function and associated Legendre polynomials.

Two fundamental Inherent Optical Properties (IOPs) of seawater are the Absorption (a) (m^{-1}) Coefficient and Volume Scattering Function (VSF) $\beta(\theta, \lambda)$ (m^{-1} sr^{-1}) – the ratio of the scattered light intensity (W/Sr) to the incident irradiance (W/m^2) per unit volume (m^3)). The other important IOPs are total scattering (b), backscattering (b_b) and

beam ($c = a+b$), all are expressed with units of m^{-1}. The VSF and scattering coefficients are defined as

$$\beta(\theta, \lambda) = \frac{1}{2}[i_1(\cos\theta) + i_2(\cos\theta)] \quad (1)$$

$$b = 2\pi \int_0^{\pi} \beta(\theta, \lambda) \sin\theta \, d\theta \quad (2)$$

where

$$i_1(\cos\theta) = \left| \sum_{n=1}^{\infty} \frac{2n+1}{n(n+1)} [a_n \pi_n(\cos\theta) + b_n \tau_n(\cos\theta)] \right|^2 \quad (3)$$

$$i_2(\cos\theta) = \left| \sum_{n=1}^{\infty} \frac{2n+1}{n(n+1)} [a_n \tau_n(\cos\theta) + b_n \pi_n(\cos\theta)] \right|^2 \quad (4)$$

where π_n and τ_n are angular dependent functions expressed in terms of Legendre polynomials and a_n and b_n are Mie coefficients in terms of Riccatti-Bessel functions [13]. In the present work, calculations of the bubbles are performed with an efficient code for the Lorenz-Mie theory.

B. THE OPTICAL PROPERTIES OF BUBBLES IN SEAWATER

Air bubbles entrained by breaking waves at the ocean surface are distinguished by their sources and characteristics as clean bubbles and coated bubbles. The number density of bubbles depends on wind speed. Measurements and models in previous studies have confirmed the bubble size distributions typically following a power law distribution with mean slope values (α) ranging from 3.6 to 4.6 [8], [29] and an average mean slope value of 4 [36], [37]. The bubble size distribution is given by

$$p(r) \propto r^{-\alpha} \quad (5)$$

where r is the radius of a bubble and α is the (dimensionless) slope of the size distribution for bubbles.

In this study, we have confined the distribution between and corresponding to the minimum and maximum bubble sizes (r_{min} and r_{max}) and bubble size distribution slopes (α). Accordingly, the above expression (Eq. 5) is rewritten in the form

$$p(r) \propto r^{-\alpha}; r_{min} < r < r_{max} \quad (6)$$

It was observed based on Mie theory simulations that the VSF is least affected by the larger bubble size, while the smaller bubble size and the distribution slope are more affected. For the VSF inversion, the power-law function for estimation of bubble size distributions is built based on the three parameters, r_{min}, r_{max} and α.

Based on measurement data reported in the literature [7], [38], the minimum and maximum radii of the bubble population are considered as 5-20 μm and 100-200 μm respectively. The absorption coefficient (a) is negligible for the clean bubbles and sufficiently lower for the coated bubbles than that for the particles. The VSF at the small forward angles is nearly unchanged for the coated bubbles when compared to that for the clean bubbles. The VSF at the backward scattering angles changes less significantly as bubble coating thickness increases, which is out of the scope of this study. Thus, the present study aimed to analyze the effect of r_{min}, r_{max} and α on the VSF, and to develop an inversion method for the determination of these parameters and clean bubble size distributions in oceanic water.

C. THE EFFECT OF r_{min} ON VSF

Air bubbles exhibit a distinctive feature near the critical-scattering angle and this feature can be described as a function of the bubble size, refractive index, and wavelength. When an air bubble in seawater is illuminated by an electromagnetic plane wave, the Mie theory gives excellent prediction for the critical angle scattering pattern (in the form of oscillations), with coarse structures characterized by dark and bright fringes superimposed on fine structures (described by high frequency and low amplitude fringes) [39]. The comparison of the scattering patterns near the critical angle showed that the main (first) peak occurs on the lower side of the critical angle (82.84°) and corresponds to the first maxima, bright fringe I_1' and its angular position θ_1' The first minima from the first central bright fringe is the first dark fringe as denoted by I_1 and θ_1. This feature is then followed by the second bright fringe with I_2' and θ_2' (Fig. 1). The main bubble characteristic which affects angular scattering is the prominent (high) scattering feature near the critical angle (around 50° to 80°) caused by the total internal reflection. This elevated scattering feature becomes less pronounced with a smaller (minimum) mean bubble size of less than 4 μm. Thus, the present study considered the minimum bubble size of 5 μm. Fig. 1 shows the effect of the minimum radius (r_{min}) of the bubble population on the VSF as described by the power law distribution function. Results from Mie calculations showed that the properties of a critical scattering pattern of visible light can be accurately modelled by bubbles

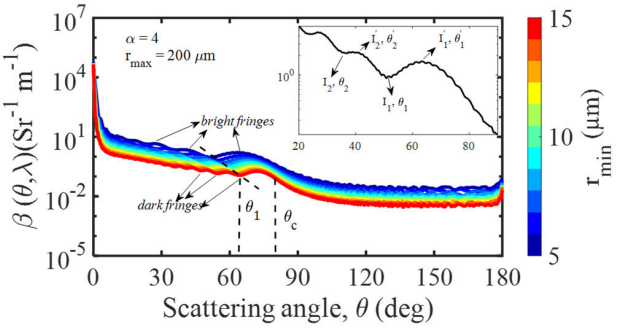

FIGURE 1. The effect of r_{min} on the volume scattering function (VSF) of bubbles in water as determined from Mie theory simulations. The bubble size distribution follows a power law function based on the fixed slope and fixed maximum bubble size. Insert shows the angular position and intensity of bright and dark fringes.

with minimum bubble size, refractive index, and size distribution slope. These results further showed that the angular position of the dark and bright shifts in the direction of the critical-scattering angle with increasing minimum bubble sizes and the angular translation takes place in a direction of the critical-scattering angle as the relative refractive index (n_i/n_m) becomes smaller. As can be seen in Fig. 1, the angular position of the first dark fringe (θ_1) shifts in a direction of the critical angle as the minimum bubble sizes increase with a large population of bubbles. Based on the analysis of the bubble scattering behavior/features near the critical angle, a new formula was derived to determine the angular distribution (position) of the first dark fringe using the results from Mie calculations and earlier studies by Marston and his co-workers. Accordingly, the intensity of the fringe pattern and position is inversely proportional to the square root of the minimum bubble size and depends on the refractive index and wavelength of the incident light. Marston and co-workers [39] derived an expression for angular spread ($\theta_c - \theta_1$) of the scattering pattern for a single bubble immersed in water.

Here, the formula of Marston and co-workers [39] is modified for the bubble population in seawater. Prediction accuracy of the modified formula was evaluated using the root mean squared error (RMSE) and other matrices. The modified formula (Eq. 7) yielded a relatively low error (RMSE 0.44) as compared to the Marston and co-workers [39] formula (RMSE = 1.03). Results showed that the angular position of the first dark fringe strongly depends on the minimum bubble size (r_{min}) and weakly on the other parameters. The angular position of the first dark fringe is

$$\theta_1 = \theta_c \left(1 - \frac{1}{m}\sqrt{\frac{\lambda}{1.22 \times r_{min}}}\right) \tag{7}$$

where λ is the wavelength of the incident light, θ_c is the critical-scattering angle (82.84°), θ_1 is the angular position of the first dark fringe, and m is the relative refractive index ($m = \frac{n_i}{n_w}$, $n_i = 1.0003$ and $n_m = 1.33257$). Fig. 2 shows the results in terms of angular position (θ_1) based on the Mie scattering theory and the new formula for various bubble sizes (approximated by a power law distribution and the relative refractive index $m = 0.75$).

D. THE EFFECT OF SIZE DISTRIBUTION SLOPE (α) ON VSF

The effect of bubble size distribution slopes on the VSF for the minimum and maximum values of bubble size is shown in Fig. 3. It can be seen that for a range of bubble size distribution slopes, the VSF of bubbles in water exhibits similar but distinctive scattering patterns over the full angular range (0-180°), which allows an accurate measure of the light scattering intensities in the position of the first dark (θ_1) and bright ($\boldsymbol{\theta'_1}$) fringes.

The results shown in Fig. 4 reveal that the ratio $\frac{I(\theta'_1)}{I(\theta_1)}$ increases with increasing bubble size distribution slopes,

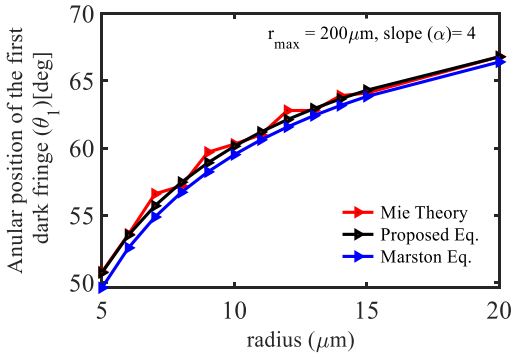

FIGURE 2. The angular position of the first critical dark fringe (θ_1) for the minimum bubble sizes of a bubble population. Results are compared with the Mie theory and Marston and co-workers' formulations.

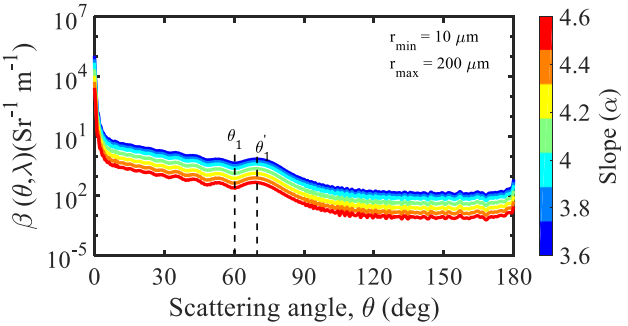

FIGURE 3. The effect of the bubble size distribution slope (α) on the volume scattering function (VSF) of the bubble population in water is determined from the results of Mie-theory-based simulations. The bubble size distribution is described by a power law function with the fixed maximum and minimum bubble sizes.

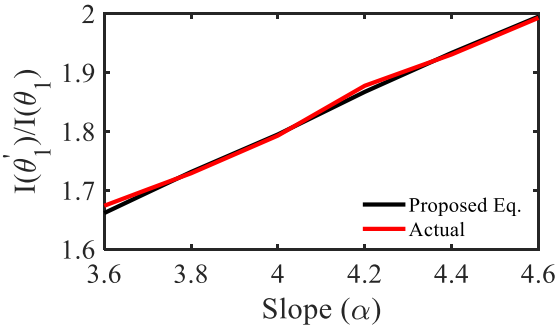

FIGURE 4. The relationship of the intensity ratio, $\frac{I(\theta'_1)}{I(\theta_1)}$ versus bubble size distribution slopes.

where θ'_1 and θ_1 are angular positions of the first critical bright and dark fringes and $I(\theta'_1)$, $I(\theta_1)$ are scattered intensities of the bright and dark fringes respectively. From the scattered intensity ratio an expression for estimating slopes of a power law distribution is derived using the results of Mie-theory-based simulations

$$\frac{I(\theta'_1)}{I(\theta_1)} = 0.95 \times \alpha^{0.6} \times r_{min}^{0.09} \tag{8}$$

E. THE EFFECT OF r_{max} ON VSF

Power law distributions of bubbles in a population with varying maximum bubble sizes exhibit small changes in the forward direction and large changes in the backward direction (Fig. 5).

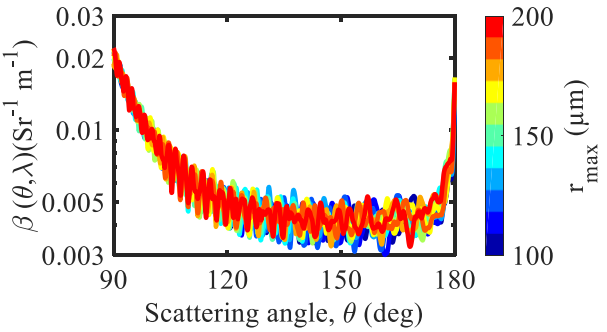

FIGURE 5. The effect of r_{max} on the VSF in the forward and backward directions for the bubbles in water based on the results of Mie-theory -based simulations. The bubble size distribution is described by a power law function with the fixed slope ($\alpha = 4$) and minimum bubble size ($r_{min} = 10$ μm).

From the results of Mie-theory-based simulations, the intensity ratio $\frac{I(82.8°)}{I(0.09°)}$ for the critical angle (82.84°) and near forward angle (≈0.09°) was calculated using the average bubble size distribution slope of 4. The $\frac{I(82.8°)}{I(0.09°)}$ decreases with increasing maximum bubble sizes and with power-law slope. This change is expressed as

$$\frac{I\,(82.8°)}{I\,(0°)} = 3 \times 10^{-4} \times (r_{min})^{-1.5} \times (r_{max})^{-0.34} \qquad (9)$$

where r_{min} and r_{max} are expressed in micrometers (μm).

The scattering (b) and backscattering coefficients (b_b) of bubble populations estimated with Mie theory and the power-law distribution showed that bubble backscattering coefficients slightly increase with increasing maximum bubble sizes (r_{max}) in the population and decrease with increasing bubble size distribution slopes (α).

III. RESULTS AND DISCUSSION

A. THEORETICAL VALIDATION

For the computation of the radiation scattering patterns, the Mie theory calculations for randomly-distributed spherical bubbles with the effects of negligible absorption (considering the imaginary part of the refractive index as negligible) and multiple scattering were performed at 515 nm reference wavelength using volume scattering function data. The results of the new formula (the proposed inversion method) were verified by comparison with those of Mie theory using the root mean square error (RMSE, $(\bar{e}) = \sqrt{\frac{1}{N}\sum(y-\bar{y})^2}$) and deviation ($(\mathbf{\Delta}) = |y-\bar{y}|$) (where N is the number of samples, y is the true value from the Mie calculations, and $\bar{y}$ is the predicted value from the new models).

The new formula inverted VSFs to infer bubble size distributions as a function of the slope, maximum and minimum bubble sizes. The bubble size distribution in ocean depends on wind speed through a power law function as considered in the present study. Based on the angular scattering structure seen in the VSF, simulations were run for the power-law distribution of bubbles with different combinations of their properties (r_{min} 5 to 20 μm with 1 μm interval, r_{max} 100 to 200 μm with 10 μm interval, and size distribution slope 3.6 to 4.6 with an increment of 3.6, 3.7, 3.8, 4.0, 4.2, 4.4, 4,6, and relative refractive index 0.75). Consequently, bubbles size distributions were derived from their scattering properties at the near forward angles and critical-scattering angle. The prominent peak in the VSF at the critical angle for bubbles was near 82.84°. This was assessed with 850 (16 × 11 × 7) samples used in the present study.

1) ESTIMATION OF r_{min}, r_{max} AND BUBBLE SIZE DISTRIBUTION SLOPES

The inverse calculations were performed for 850 samples of bubble population following the power-law distribution (Eq. 7). Predicted minimum bubble sizes have the highest accuracy with a root mean square error ($\bar{e}_{r_{min}}$) of 0.33 μm, which indicates a good prediction of the minimum bubble sizes in a given distribution. The minimum bubble is an important parameter for determining the scattering coefficient and number density of bubbles [7]

$$b = 3\pi \times Q_s \times N_0 \times r_{min}^2 \qquad (10)$$

where b is the scattering coefficient, Q_s is the scattering efficiency and N_0 is the number density of bubbles

Fig. 6 shows the relative error ($\Delta r_{min}/r_{min}$) between predicted minimum bubble sizes and known bubble sizes for the constant slope valu ($\alpha = 4$) with the changes in maximum bubble sizes. As can be seen, the inverse results agree well with Mie theory simulations in terms of predicting minimum bubbles sizes with a RMSE of 0.33 μm and a mean error of 0.27 μm.

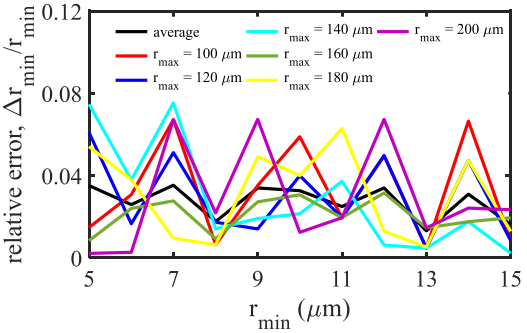

FIGURE 6. The relative error ($\Delta r_{min}/r_{min}$) between predicted minimum bubble sizes (from inverse results) and known bubble sizes. The black solid line represents the mean deviation for all samples.

Using the inverse results (Eqs. 8 and 9), bubble size distribution slopes and maximum bubble sizes were estimated. Fig. 7 shows the relative error ($\Delta r_{max}/r_{max}$) between predicted maximum bubble sizes and known maximum bubble sizes. The maximum bubble size has a less significant effect

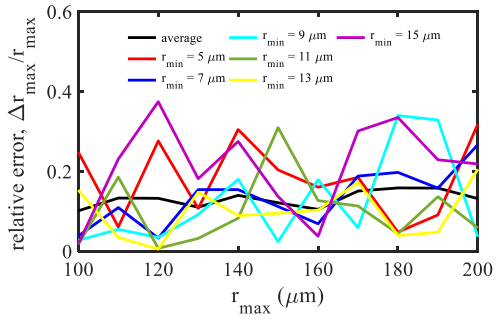

FIGURE 7. The relative error ($\Delta r_{max}/r_{max}$) between predicted maximum bubble sizes and known bubble sizes with the size distribution slope of 4. The black solid line represents the mean deviation for all the samples.

on the volume scattering function of bubble populations, especially when the size distribution slope is higher than 4. For prediction of the mean size distribution slope (α =4), good accuracy was achieved for maximum bubble sizes with a mean deviation of 20 μm. It should be noted that the proposed method (Eq. 8) is a function of the minimum bubble sizes (as described previously) and intensity ratio $\left(\frac{I(\theta_1')}{I(\theta_1)}\right)$, which increases linearly with the size distribution slope values.

Fig. 8 shows the predicted slopes with the minimum and maximum bubble sizes in a bubble population. The predicted

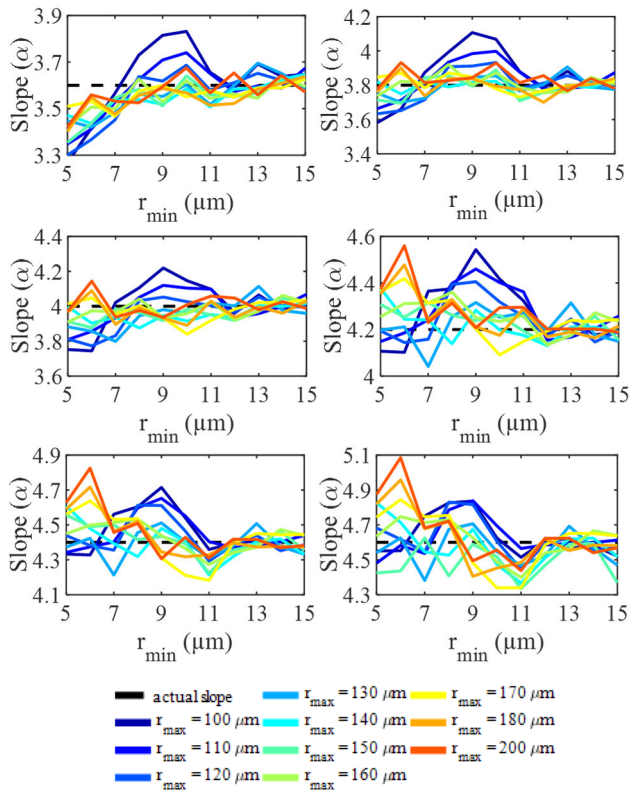

FIGURE 8. Comparison of the predicted and known bubble size distribution slopes for the minimum and maximum bubble sizes with the power-law distribution. The black line in each sub-plot represents the known bubble size distribution slopes.

slopes generally agree well with known slopes for the minimum bubble sizes greater than 8 μm. When the slope is smaller (less than 4), the predicted slopes are underestimated. The error in the prediction of slopes is 0.18 (RMSE) and 0.12 (mean deviation).

In this study, a model for bubble size distribution was developed that considers the above parameters. Results are presented for several cases of the bubble sizes (Fig. 9). This validation confirms that predicted bubble size distributions are in good agreement with known bubble distributions for various bubble populations.

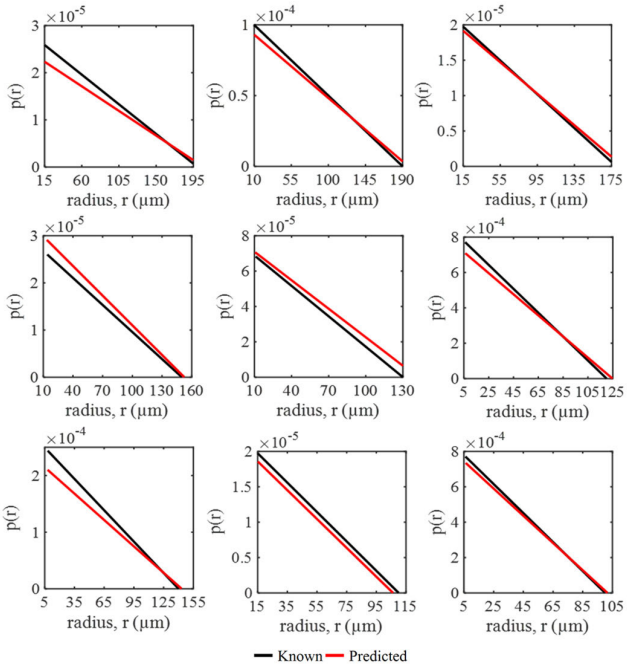

FIGURE 9. Comparison of the predicted and known bubble size distributions with slope $\alpha = 4$. Black and red solid lines indicate the known and predicted bubble size distributions.

2) RELATIONSHIP IN THE PHASE FUNCTIONS ($\tilde{\beta}(\theta\lambda)$) BETWEEN THE NORMAL AND POWER-LAW DISTRIBUTED BUBBLES

In this work, a relationship in the scattering phase functions ($\tilde{\beta}(\boldsymbol{\theta}, \boldsymbol{\lambda})$) of bubbles between power-law and normal distributions was developed and its results were compared with laboratory experiments data for the realistic ocean bubble populations. Note that the angular positions of the first critical dark fringe depend on the mean bubble size in the normal distribution and minimum bubble size in the power-law distribution.

Fig. 10 shows the scattering phase functions of bubbles exhibited by power-law and normal distributions with the minimum bubble size ($\boldsymbol{r_\theta}$) and constant slope (α). It is seen that the scattering phase functions of the bubbles with the power-law distribution closely match the results predicted with the normal distribution (with the mean bubble size $\boldsymbol{r_\theta \times 122}$ and any value of standard deviation (σ)).

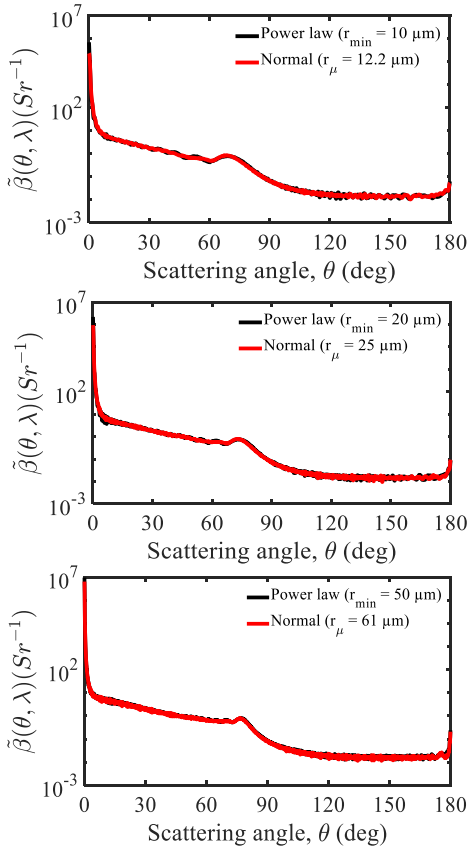

FIGURE 10. Scattering phase functions ($\tilde{\beta}(\theta, \lambda)$) exhibited by power-law and normally-distributed bubble populations with different sizes (slope (α) = 4 and standard deviation (σ) = 10% of mean).

The primary focus of this study is in the vicinity of the critical-angle region (50-82.84°), thus the above results are important as the phase function close to the critical angles is independent of the standard deviation in the normal distribution and of the slope in the power law distribution.

B. EXPERIMENTAL RESULTS

This section presents a comparison of the simulation results with the measurement data, which were obtained from laboratory experiments using a LISST VSF meter. The LISST VSF meter is a submersible multi-angle polarized light scattering meter and consists of 32 ring detectors and a rotating eye ball. The ring detectors are used to sense light scattered by bubbles in the near-forward angles (0.094-15°, with very high resolution) and a rotating eye ball to measure the scattering intensity at other (larger) angles (with 1° resolution) [40]. The instrument uses the ring detector with a single 515 nm TE-cooled diode laser with a longer path length. The experiments were carried out in a glass tank with dimensions 160 cm × 60 cm × 60 cm. The experimental set-up (shown in Fig. 11) includes the bubble generators and a VSF meter. The tank was filled with deionized water (with no particulates) to a depth of 30 cm. The air bubbles were generated by three different (pore size) diffusers with the dimensions

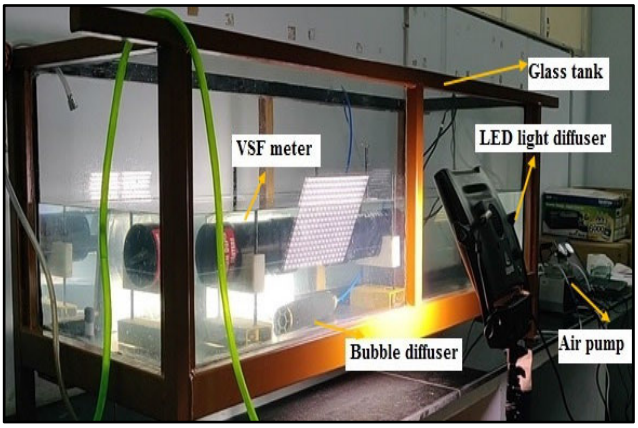

FIGURE 11. The laboratory experimental setup for bubble generation and measurements in water using a VSF meter.

of 30 cm length and 3 cm radius. The bubble diffusers were placed at the bottom of a glass tank and air pressure was applied at one end of the diffuser and gas was injected at another end to control and drive air with a constant flow rate for generating small bubbles.

The bubbles generated near the bottom of the tank rose through the water at a uniform speed. A high-speed camera and an image acquisition software recorded the bubble motion. A LED light was placed for good illumination and a reference scale was immersed in water for measuring the bubble size. When the diffusers generated bubbles, it was difficult to capture all bubbles in the image. Thus, a small section of the bubble image was acquired and analyzed for the determination of the bubble size distribution in laboratory conditions.

Three diffusers were used with the average pore size of 50, 20, 10 μm. Each diffuser produced bubbles with respect to the air flow rate per unit length. Based on the analysis of the captured images, bubble populations produced by three diffusers are categorized into three size fractions: Test-1 bubbles > Test-2 bubbles > Test-3 bubbles. Small sections of the images of bubbles produced by three different diffusers are shown in Fig. 12. The minimum bubble sizes measured were 50, 20, 10 μm respectively.

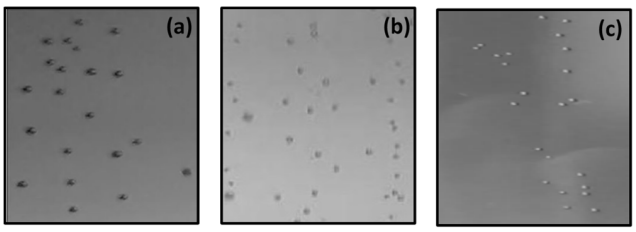

FIGURE 12. Sections of the images of bubbles categorized into three size fractions: (a) Test-1 > (b) Test-2 > and (c) Test-3 types of bubbles based on their size. For comparison purposes, these images were produced with the same scale.

Volume scattering functions of the bubbles in the tank experiment were measured with the multi-angle polarized

light scattering meter (LISST VSF meter). Experimental results showed that generated bubble size distributions typically followed a normal distribution, whereas bubbles entrained by mechanically generated breaking water surface waves were log-normally distributed. Our results from the new inversion method of bubble size distribution based on the experimental data showed that angular positions of the first critical dark fringe shift in the direction of the critical angle as the size of the bubble increases. This observation is well consistent with theoretical predictions wherein angular position (θ_1) shifts occurred for the bubble populations characterized by the normal, log normal or power-law distributions.

Fig. 13 shows laboratory observations of the VSFs for bubbles as categorized into three sizes. The laboratory measurements (for the normally-distributed bubbles) have confirmed our theoretical predictions (for the power-law distributed bubbles) of elevated scattering feature and angular position shifts near the critical angle. These results suggest that the proposed inversion method is a power tool for predicting the bubble size distribution in seawater. The inversion parameters associated with the proposed formula are described in Table 1.

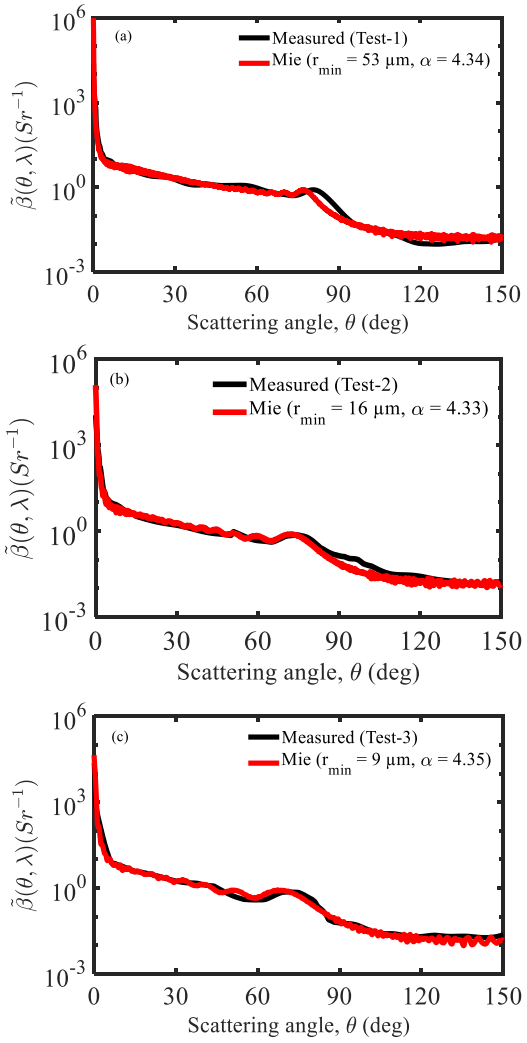

FIGURE 13. Comparison of the laboratory measurements with theoretical predictions (using the Mie theory) of the phase functions ($\tilde{\beta}(\theta,\lambda)$) for the bubble populations of three size classes. (a) Test-1, (b) Test-2, and (c) Test-3.

TABLE 1. The inversion parameters used for determining the bubble size distribution in seawater using the proposed method.

Experiment	θ_1	r_{min} (Photography)	r_{min} (Inverse VSF)	$\frac{I(\theta_1')}{I(\theta_1)}$	α (slope)
Test-1	59	10	9	1.88	4.35
Test-2	65	19	16	1.78	4.33
Test-3	73	50	53	1.60	4.34

The new inversion method presented here is used to study the influence of bubbles on the VSFs in seawater. This, present study is unique in its approach and the results have significant implications for the subsea optical communication/imaging studies and remote sensing of the ocean colour. The present study also forms the basis for a detailed investigation of the ocean water composed of other substances in addition to the bubbles, which is our future work. The limitation of the present study is its applicability to the bubble VSFs (obtained by subtraction of VSFs by water molecules and particulates).

IV. CONCLUSION

This study presented the important results on the light scattering patterns of the oceanic bubble populations near the critical angle using Mie theory simulations and laboratory experimental data. Simulations were conducted with varying bubble size distributions (in the range from 5 to 200 μm). Small deeply penetrating bubbles and those produced by breaking surface waves typically followed the power-law and normal distributions. A relationship in the VSFs between these two bubble size distributions was established. Simulations and experimental results showed that the angular position of the critical dark fringe shifts in the direction of the critical angle as the minimum bubble size increases. The intensity ratio of the bright to dark fringes increased with the slope of the size distribution for bubbles and the intensity ratio of the critical angle to near forward angle decreased with increasing maximum bubble sizes with a power-law function. Using these data, an inversion method was developed to derive the bubble size distribution (r_{min}, r_{max} and α) in seawater. Model predictions agreed well with the simulation (Mie theory) results. Experimental results have confirmed a transition in the angular position of the first critical dark fringe and the intensity ratios with increasing mean bubble sizes. An evaluation of the applicability and accuracy of the new inversion method using simulations and experimental results revealed that the proposed inversion method gives a very good approximation of the bubble size distribution as described by a power-law function with bubble sizes ranging from 5 to 200 μm and

slope values ranging from 3.6 to 4.6. The results presented here have significant implications for the remote sensing of ocean colour, subsea optical investigations, underwater imaging, and underwater wireless optical communications.

REFERENCES

[1] R. Sahoo, S. K. Sahu, and P. Shanmugam, "Estimation of the channel characteristics of a vertically downward optical wireless communication link in realistic oceanic waters," *Opt. Laser Technol.*, vol. 116, pp. 144–154, Aug. 2019, doi: 10.1016/j.optlastec.2019.03.023.

[2] J. Piskozub, D. Stramski, E. Terrill, and W. K. Melville, "Small-scale effects of underwater bubble clouds on ocean reflectance: 3-D modeling results," *Opt. Exp.*, vol. 17, no. 14, Jul. 2009, Art. no. 11747, doi: 10.1364/oe.17.011747.

[3] B. Yan, B. Chen, and K. Stamnes, "Role of oceanic air bubbles in atmospheric correction of ocean color imagery," *Appl. Opt.*, vol. 41, no. 12, p. 2202, Apr. 2002, doi: 10.1364/ao.41.002202.

[4] E. Lamarre and W. K. Melville, "Air entrainment and dissipation in breaking waves," *Nature*, vol. 351, no. 6326, pp. 469–472, Jun. 1991, doi: 10.1038/351469a0.

[5] S. A. Thorpe and P. N. Humphries, "Bubbles and breaking waves," *Nature*, vol. 283, no. 5746, pp. 463–465, Jan. 1980, doi: 10.1038/283463a0.

[6] W. H. Munk, P. Scully-Power, and F. Zachariasen, "The Bakerian lecture, 1986 ships from space," *Proc. R. Soc. A Math. Phys. Eng. Sci.*, vol. 412, no. 1843, pp. 231–254, Aug. 1987, doi: 10.1098/rspa.1987.0087.

[7] L. Ma, F. Wang, C. Wang, C. Wang, and J. Tan, "Monte Carlo simulation of spectral reflectance and BRDF of the bubble layer in the upper ocean," *Opt. Exp.*, vol. 23, no. 19, p. 24274, Sep. 2015, doi: 10.1364/oe.23.024274.

[8] K. Randolph, H. M. Dierssen, M. Twardowski, A. Cifuentes-Lorenzen, and C. J. Zappa, "Optical measurements of small deeply penetrating bubble populations generated by breaking waves in the southern ocean," *J. Geophys. Res., Oceans*, vol. 119, no. 2, pp. 757–776, Feb. 2014, doi: 10.1002/2013JC009227.

[9] K. D. Moore, K. J. Voss, and H. R. Gordon, "Spectral reflectance of whitecaps?: Their contribution to water-leaving radiance," *J. Geophys. Res., Oceans*, vol. 105, pp. 6493–6499, Mar. 2000.

[10] D. Stramski and J. Tegowski, "Effects of intermittent entrainment of air bubbles by breaking wind waves on ocean reflectance and underwater light field," *J. Geophys. Res., Oceans*, vol. 106, no. C12, pp. 31345–31360, Dec. 2001, doi: 10.1029/2000jc000461.

[11] E. J. Terrill, W. K. Melville, and D. Stramski, "Bubble entrainment by breaking waves and their influence on optical scattering in the upper ocean," *J. Geophys. Res., Oceans*, vol. 106, pp. 815–823, Aug. 2001.

[12] X. Zhang, M. Lewis, M. Lee, B. Johnson, and G. Korotaev, "The volume scattering function of natural bubble populations," *Limnol. Oceanogr.*, vol. 47, no. 5, pp. 1273–1282, Sep. 2002, doi: 10.4319/lo.2002.47.5.1273.

[13] C. F. Bohren and D. R. Huffman, *Absorption and Scattering of Light by Small Particles*. Hoboken, NJ, USA: Wiley, 1998.

[14] F. Onofri, G. Gréhan, and G. Gouesbet, "Electromagnetic scattering from a multilayered sphere located in an arbitrary beam," *Appl. Opt.*, vol. 34, no. 30, p. 7113, Oct. 1995, doi: 10.1364/ao.34.007113.

[15] J. A. Lock and G. Gouesbet, "Generalized Lorenz–Mie theory and applications," *J. Quant. Spectrosc. Radiat. Transf.*, vol. 110, no. 11, pp. 800–807, Jul. 2009, doi: 10.1016/j.jqsrt.2008.11.013.

[16] H. Czerski, M. Twardowski, X. Zhang, and S. Vagle, "Resolving size distributions of bubbles with radii less than 30 μm with optical and acoustical methods," *J. Geophys. Res., Oceans*, vol. 116, no. C7, pp. 1–13, Jul. 2011, doi: 10.1029/2011JC007177.

[17] H. Groundwater, M. S. Twardowski, H. M. Dierssen, A. Sciandra, and S. A. Freeman, "Determining size distributions and composition of particles suspended in water: A new SEM–EDS protocol with validation and comparison to other methods," *J. Atmos. Ocean. Technol.*, vol. 29, no. 3, pp. 433–449, Mar. 2012, doi: 10.1175/JTECH-D-11-00026.1.

[18] D. Stramski, R. A. Reynolds, P. Gernez, R. Röttgers, and O. Wurl, "Inherent optical properties and particle characteristics of the sea-surface microlayer," *Prog. Oceanogr.*, vol. 176, Sep. 2019, Art. no. 102117, doi: 10.1016/j.pocean.2019.05.009.

[19] T. Kawaguchi, Y. Akasaka, and M. Maeda, "Size measurements of droplets and bubbles by advanced interferometric laser imaging technique," *Meas. Sci. Technol.*, vol. 13, no. 3, pp. 308–316, Mar. 2002, doi: 10.1088/0957-0233/13/3/312.

[20] M. Krzysiek. (2009). *Particle Systems Characterization by Inversion of Critical Light Scattering Patterns*. [Online]. Available: https://tel.archives-ouvertes.fr/tel-00443983/document

[21] X. Zhang, M. Lewis, and B. Johnson, "Influence of bubbles on scattering of light in the ocean," *Appl. Opt.*, vol. 37, no. 27, p. 6525, Sep. 1998, doi: 10.1364/ao.37.006525.

[22] X. Quan and E. S. Fry, "Empirical equation for the index of refraction of seawater," *Appl. Opt.*, vol. 34, no. 18, p. 3477, Jun. 1995, doi: 10.1364/ao.34.003477.

[23] R. W. Austin and G. Halikas, "The index of refraction of seawater," *SIO Ref.*, vol. 1, p. 124, Jan. 1976. [Online]. Available: http://oai.dtic.mil/oai/oai?verb=getRecord&metadataPrefix=html&identifier=ADA024800

[24] E. M. Stanley, "The refractive index of seawater as a function of temperature, pressure and two wavelengths," *Deep. Res. Oceanogr. Abstr.*, vol. 18, no. 8, pp. 833–840, 1971, doi: 10.1016/0011-7471(71)90050-7.

[25] X. Zhang, M. Lewis, W. P. Bissett, B. Johnson, and D. Kohler, "Optical influence of ship wakes," *Appl. Opt.*, vol. 43, no. 15, pp. 3122–3132, 2004, doi: 10.1364/AO.43.003122.

[26] M. E. Lee and M. R. Lewis, "A new method for the measurement of the optical volume scattering function in the upper ocean," *J. Atmos. Ocean. Technol.*, vol. 20, no. 4, pp. 563–571, Apr. 2003.

[27] H. J. B. Couto, D. G. Nunes, R. Neumann, and S. C. A. França, "Micro-bubble size distribution measurements by laser diffraction technique," *Minerals Eng.*, vol. 22, no. 4, pp. 330–335, Mar. 2009, doi: 10.1016/j.mineng.2008.09.006.

[28] H. Kobayashi, S. Maeda, M. Kashiwa, and T. Fujita, "Measurements of ultrafine bubbles using different types of particle size measuring instruments," in *Proc. Int. Conf. Opt. Part. Characterization (OPC)*, Aug. 2014, Art. no. 92320U, doi: 10.1117/12.2064638.

[29] S. Husin, A. Addali, and D. Mba, "Acoustic frequency for bubble size correlation using acoustic emissions," *WIT Trans. Eng. Sci.*, vol. 74, pp. 414–425, Feb. 2012, doi: 10.2495/AFM120371.

[30] S. Wang, Y. Zhang, J. C. Meredith, S. H. Behrens, M. K. Tripathi, and K. C. Sahu, "The dynamics of rising oil-coated bubbles: Experiments and simulations," *Soft Matter*, vol. 14, no. 14, pp. 2724–2734, 2018, doi: 10.1039/c7sm01603d.

[31] S. Vagle and D. M. Farmer, "A comparison of four methods for bubble size and void fraction measurements," *IEEE J. Ocean. Eng.*, vol. 23, no. 3, pp. 211–222, Jul. 1998, doi: 10.1109/48.701193.

[32] F. Onofri, M. Krzysiek, J. Mroczka, K. F. Ren, and S. Radev, "Collective critical angle scattering for bubble clouds characterization," in *Proc. 14th Int. Symp. Appl. Laser Techn. Fluid Mech.*, Jun. 2008, pp. 7–10.

[33] F. R. A. Onofri, J. Worms, and M. Krzysiek, "Generalisation of the critical angle refractometry for the characterisation of clouds of bubbles," in *Proc. 13th Int. Symp. Appl. Laser Techn. Fluid Mech.*, Jun. 2006. [Online]. Available: http://ltces.dem.ist.utl.pt/lxlaser/lxlaser2006/downloads/abstracts/7.3.pdf

[34] M. Twardowski, X. Zhang, S. Vagle, J. Sullivan, S. Freeman, H. Czerski, Y. You, L. Bi, and G. Kattawar, "The optical volume scattering function in a surf zone inverted to derive sediment and bubble particle subpopulations," *J. Geophys. Res. Ocean.*, vol. 117, no. 2, pp. 1–18, 2012, doi: 10.1029/2011JC007347.

[35] X. Zhang, M. Twardowski, and M. Lewis, "Retrieving composition and sizes of oceanic particle subpopulations from the volume scattering function," *Appl. Opt.*, vol. 50, no. 9, pp. 1240–1259, 2011, doi: 10.1364/AO.50.001240.

[36] J. Wu, "Bubble populations and spectra in near-surface ocean: Summary and review of field measurements," *J. Geophys. Res.*, vol. 86, no. C1, p. 457, 1981, doi: 10.1029/jc086ic01p00457.

[37] A. L. Walsh and P. J. Mulhearn, "Photographic measurements of bubble populations from breaking wind waves at sea," *J. Geophys. Res.*, vol. 92, no. C13, p. 14553, 1987, doi: 10.1029/JC092iC13p14553.

[38] C. Wang, J. Tan, and Q. Lai, "The influence of bubble populations generated under windy conditions on the blue-green light transmission in the upper ocean: An exploratory approach," *Mod. Phys. Lett. B*, vol. 30, no. 36, pp. 1–14, 2016, doi: 10.1142/S0217984916504200.

[39] P. L. Marston, D. S. Langley, and D. L. Kingsbury, "Light scattering by bubbles in liquids: Mie theory, physical-optics approximations, and experiments," *Appl. Sci. Res.*, vol. 38, no. 1, pp. 373–383, 1982, doi: 10.1007/BF00385967.

[40] L. Hu, X. Zhang, Y. Xiong, and M.-X. He, "Calibration of the LISST-VSF to derive the volume scattering functions in clear waters," *Opt. Exp.*, vol. 27, no. 16, Aug. 2019, Art. no. A1188, doi: 10.1364/oe.27.0a1188.

BHOGESWARA RAO ANGARA received the B.Tech. degree in electronics and communication engineering (ECE) from Andhra University, Andhra Pradesh, India, in 2011, and the M.Tech. degree in control and instrumentation from Delhi Technological University (DTU), Delhi, India, in 2015. He is currently pursuing the Ph.D. degree with the Department of Ocean and Electrical Engineering, IIT Madras, Chennai, India. His research interest includes underwater wireless optical communications (UWOC).

PALANISAMY SHANMUGAM received the Ph.D. degree in optical/microwave remote sensing techniques from Anna University, Chennai, India, in 2002.

He has been a Principal Investigator of several projects funded by the Government of India. He is currently a Professor with the Department of Ocean Engineering, IIT Madras, Chennai, where he is involved in the experimental and theoretical studies of the optical properties of natural waters, air–sea interface, and subsea optical processes. His current research interests include developing models for ocean optical studies and retrieval algorithms for multispectral and hyperspectral remote sensing sensors with an emphasis on applications to sediment dynamics, algal blooms, climate change, and marine environmental and coastal processes.

HARISHANKAR RAMACHANDRAN received the B.Tech. degree in electrical engineering from IIT Bombay, in 1982, and the Ph.D. degree in electrical engineering from the University of California at Berkeley.

He was a Research Scientist with the Physics Department, University of California, Los Angeles, for five years before returning to India. He was a Scientist at the Institute for Plasma Research, Gandhinagar, from 1993 to 2001. He joined IIT Madras, in November 2001. He is currently a Professor with the Department of Electrical Engineering, IIT Madras. His research interests includes optical link design and planning, nonlinear optics, computational optics, edge plasma physics, and computational plasma physics.